Ferroelectricity from coupled cooperative Jahn-Teller distortions and octahedral rotations in ordered Ruddlesden-Popper manganates

Antonio Cammarata and James M. Rondinelli

Phys. Rev. B **92**, 014102 — Published 2 July 2015

DOI: 10.1103/PhysRevB.92.014102

Ferroelectricity from Coupled Cooperative Jahn-Teller Distortions and Octahedral Rotations in Ordered Ruddlesden-Popper Manganates

Antonio Cammarata*
Department of Control Engineering, Czech Technical University in Prague, Technicka 2, 16627 Prague 6, Czech Republic

James M. Rondinelli†
Department of Materials Science and Engineering, Northwestern University, Evanston, IL 60208, USA

(Dated: May 5, 2015)

Density functional theory and group theoretical methods are used to explore the origin for ferroelectricity in cation ordered $LaSrMnO_4$ with the Ruddlesden-Popper structure. The equilibrium phase exhibits the polar, $Pca2_1$ space group, where small polar displacements of d^4 Mn^{3+} coexist with antiferrodistortive octahedral rotations and Jahn-Teller distortions. We find that the octahedral rotations and Jahn-Teller distortion stabilize the polar structure and induce polar displacements through high-order anharmonic interactions among the three modes, making $LaSrMnO_4$ a hybrid-improper ferroelectric material. The rotations result from the ionic size mismatch between the A cations and Mn whereas the Jahn-Teller distortions are energetically favored owing to the coupling between the local e_g orbital polarization of the two nearest neighboring Mn cations in the two dimensional MnO_2 sheets. Our results indicate that anharmonic interactions among multiple centric modes can be activated by cation ordering to induce polar displacements in layered oxides, making it a reliable approach for realizing acentric responses in artificially constructed materials.

PACS numbers: 31.15.A-, 61.50.Ah, 77.80.B-, 61.50.-f

I. INTRODUCTION

Multiferroic materials with coexisting magnetic order and ferroelectric polarization have attracted intense research attention, because they provide a platform for multifunctional devices if magnetic spins can be controlled by applied voltages through magnetoelectric interactions.[1,2] The challenging aspect of discovering materials with these properties is due to the two apparently contrasting microscopic origins for the ferroic order parameters, *i.e.*, magnetism and ferroelectricity often appear to be mutually exclusive in a single phase materials.[3,4] The former usually necessitates covalent bond formation between oxygen and a transition metal with empty d states, which precludes moment formation from unpaired electron spins in the d manifold.[5]

When an electric polarization P is the result of a more complex, often termed 'improper', mechanism than a proper polar instability, magnetic order and spontaneous electric polarizations can coexist as the chemical restrictions on the cations undergoing the polar displacements are removed. Proposed improper mechanisms based on electronic degrees of freedom include magnetic cycloidal order,[6] charge ordering,[7] and spin-Peierls distortions.[8] More recently several (hybrid) improper ferroelectric mechanisms have been proposed that rely on lattice anharmonicities between two or more displacive modes (Q) of the crystal,[9–12] Useful anharmonicities in the free energy potential are of the form $\lambda P^n Q^m, \lambda P^n Q_1^m Q_2^\ell, \ldots$, where n, m, ℓ is an integer less than or equal to 3 that depends on the symmetry of the crystal, and λ is the coupling coefficient. The combination of multiple, nominally centric, Q lattice distortions may then couple together to remove inversion symmetry and produce an electric polarization,[13–15] owing to the presence of specific cation orderings.[16] Since the polarization arises from intrinsic instabilities of the lattice, magnetism and ferroelectricity can coexist by selecting magnetic cations that when in a suitable crystalline structure exhibit similar phonon dispersions (Q-modes) and hence will also support an electric polarization.[17–19]

Octahedral rotation modes in perovskite-structured oxides are key candidate lattice modes to couple together because they influence the magnetic properties of many materials.[20–22] They also couple to first-order Jahn-Teller (FOJT) lattice distortions,[23–25] but normally the combination of a tilt mode and FOJT mode, which is driven by an electronic degeneracy, will always maintain inversion unless additional symmetry reductions are achieved.[26] This concept was recently explored in metal-organic framework structures exhibiting the perovskite topology with FOJT-active transition metal ions,[27,28] and a symmetry-allowed trilinear energy term coupling a Jahn-Teller lattice distortion (Q_1) with a molecular rotation (Q_2) emerged. This anharmonic interaction induces both an electric polarization and a reasonable magnetoelectric response, owing to antiferromangetic ordering that is sensitive the antiferrodistortive Jahn-Teller pattern. Intriguingly, the number of inorganic oxides which exhibit ferroelectricity induced by this anharmonic interaction are scarce,[26,29] but it remains unclear whether that fact stems from limitations on the available coupling terms and coefficients, or rather that 'missing yet stable compounds' with such coupling have not been synthesized.[30]

In this work we design A-cation ordered $LaSrMnO_4$ with the layered $n = 1$ Ruddlesden-Popper (RP) structure

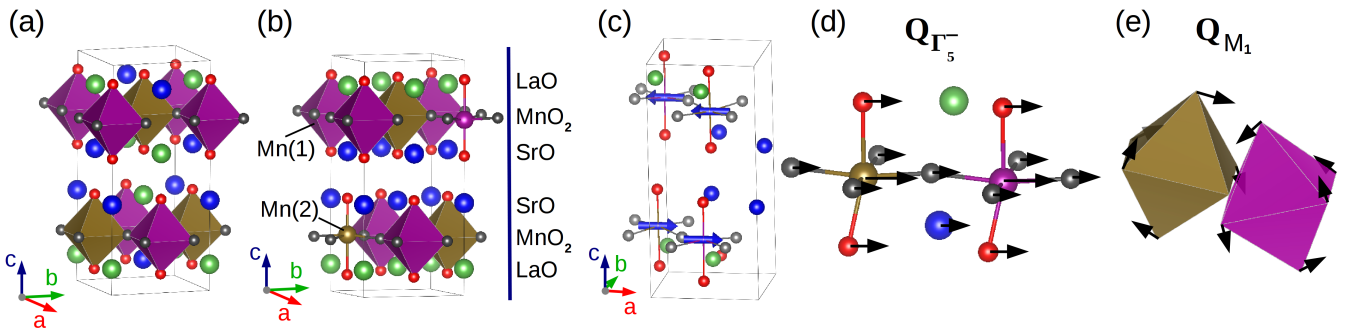

FIG. 1. (a) $LaSrMnO_4$ structure with random occupancy of La and Sr on the A site. (b) Layered cation ordered $LaSrMnO_4$ structure with subsequent monoxide LaO and SrO planes alternating along the c axis. (c) Schematic of the collinear A-type antiferromagnetic structure. (d) Polar ($Q_{\Gamma_5^-}$) and (e) rotation (Q_{M_1}) distortions present in the ground phase; (black) arrows indicate the relative atomic directions displacements. In all panels, gray and red spheres correspond to the equatorial and apical oxygen atoms coordinating Mn, respectively.

and show that ferroelectricity emerges as a consequence of anharmonic coupling between a first-order Jahn-Teller distortion and octahedral rotations. Although such RP manganates have been explored before in bulk as solid-solutions, we show that ordering of La and Sr in a layered fashion is a prerequisite to activate the anharmonic coupling that stabilizes the polar $Pca2_1$ phase. We show that the hybrid-improper ferroelectricity arises from the coupling of the distinct e_g orbital polarizations of two nearest neighbor Mn sites in combination with MnO_6 octahedral rotations. Finally we explore competing magnetic ground states compatible with the polar structure.

II. MODEL & COMPUTATIONAL METHODS

Solid solution $LaSrMnO_4$ (LSMO) is found to be a Mott-Hubbard insulator,[31,32] crystallizing in the centrosymmetric $I4/mmm$ space group with antiferromagnetic ordering[33] depicted in Fig. 1a. It has recently been grown in the RP structure as a thin film with random occupancy of La and Sr on the A site.[34] Layer-by-layer growth of LSMO, however, also makes it possible to achieve desired A-cation ordered arrangements,[35,36] *i.e.*, periodic LaO and SrO monoxide planes along the crystallographic direction with disconnected MnO_6 octahedra (Fig. 1b).

Recent representation theory analyses[37] have shown that the AO monoxide layer sequence can impose key symmetry reductions, which in the presence of octahedral distortions – tilt modes and Jahn-Teller bond distortions – produce crystal structures without inversion symmetry provided that the cations are selected such that they promote the targeted displacive modes. Here we consider the monoxide layer sequence $\cdots$–[SrO|MnO_2|LaO]–[LaO|MnO_2|SrO]–$\cdots$, which has been referred to as an $\eta = 2$ superlattice[38] (Fig. 1b). [The square brackets indicate the perovskite blocks, which are interleaved to form the $n = 1$ RP phase by translating each layer by $(1/2, 1/2, 0)$]. Here, the Mn^{3+} cation with a $3d^4 : t_{2g}^3 e_g^1$ electronic configuration is always found between chemically inequivalent AO layers.

The $\eta = 2$ cation layering sequence maintains inversion symmetry in the absence of any other structural distortions, space group $P4/nmm$; therefore, we choose it as the ideal paraelectric reference phase. We also consider a periodic $\sqrt{2} \times \sqrt{2} \times 1$ (28-atom) supercell within our density functional theory (DFT) simulations as it explicitly contains four Mn atoms, which allows us to explore multiple antiferromagnetic (AFM) spin, FOJT distortion patterns, and other cell-doubling lattice distortions.

Our DFT calculations use the projector-augmented wave (PAW) formalism[39] as implemented in the Vienna *Ab initio* Simulation Package (VASP),[40] with a minimum plane-wave cutoff of 600 eV, and performed with the local-density approximation (LDA) functional plus Hubbard U method[41] (LDA+U). We chose the rotationally invariant version introduced by Liechtenstein *et al.*[42] with $U = 5.0$ eV and $J = 1.0$ eV. The Brillouin zone is sampled with a minimum of a $7\times7\times5$ k-point mesh and integrations are performed with Gaussian smearing (20 meV width). Full structural (atomic and lattice) relaxations are initiated from the ideal reference phase and the Hellmann-Feynman forces minimized to a 0.5 meV Å^{-1} tolerance. Unless otherwise notes, we consider a collinear A-type AFM order (Fig. 1c), which we found to be the lowest energy spin configuration of those surveyed.

III. RESULTS AND DISCUSSION

A. Ground State Structure

We begin by searching for the equilibrium ground state structure by computing the dynamical force constant matrix of the paraelectric phase ($P4/nmm$) and using (combinations) of unstable and soft eigendisplacements to generate probable low-symmetry phases. Following variable cell and atomic position relaxations, we find that the lowest energy structure of those surveyed to be polar and insulating with an electronic bandgap of

$\simeq 0.95\,\mathrm{eV}$. To investigate the lattice Q modes involved in the symmetry reduction to the polar $Pca2_1$ phase, we perform a group-theoretical analysis[43] of the calculated orthorhombic ground state by decomposing it into irreducible representations (irreps) of the tetragonal paraelectric phase aided by the ISODISTORT software.[44] The significant modes that appear in the ground state (with mode amplitude specified in parentheses) are: $Q_{\Gamma_1^+}$, describing Mn–O bond elongations along the c-axis (0.13 Å), Q_{M_1} out-of-phase octahedral rotations (0.30 Å), and Q_{M_4} cooperative Jahn-Teller distortions (0.15 Å). We describe them in more detail below. A smaller contribution is found for the $Q_{\Gamma_5^-}$ polar mode (0.02 Å, Fig. 1d), which contributes to the total electric polarization. Note that our group-theoretical analysis shows that the polar phase can be achieved by coupling two of any of the three – polar displacement ($Q_{\Gamma_5^-}$), octahedral rotations (Q_{M_1}) and Jahn-Teller mode (Q_{M_4}) – distortions.

The structural mode $Q_{\Gamma_1^+}$ preserves the symmetry of the paraelectric phase. It consists of La, Sr, and apical oxygen atom displacements along the c-axis. Owing to the double AO layers that separate the MnO_2 planes, the apical oxygen atoms are free to displace along the c-axis. Here we find that this mode displaces two adjacent AO layers along the c-axis and in opposite directions, which results in an elongation of the octahedra and Mn–O bonds along the c-axis. The distortion mode Q_{M_1} (Fig. 1e) reduces the $P4/nmm$ structure to the centric $Pbcm$ symmetry. It produces out-of-phase rotations of two subsequent octahedra about an axis joining two nearest neighboring Mn atoms lying in the ab-plane. Finally, the Jahn-Teller distortion Q_{M_4}, which is also referred to as the Q_2 mode in the manganate literature,[45] induces an asymmetric stretching of the Mn–O equatorial bonds.

B. Anharmonic Lattice Interactions

We next explore in detail the energetic contribution of the Q modes to stabilizing the polar structure. First, our phonon band structure calculations for the paraelectric phase reveal that only the octahedral rotation mode, Q_{M_1}, is dynamically unstable with a mode frequency of $15i\,\mathrm{cm}^{-1}$. Q_{M_4} and $Q_{\Gamma_5^-}$ modes are found to have real mode frequencies, 1381 and $139\,\mathrm{cm}^{-1}$, respectively. As noted earlier, the octahedral rotations alone cannot produce the $Pca2_1$ structure, which indicates some anharmonic interaction between the rotations and another mode is necessary to capture the symmetry reduction.

1. *Independent Distortions*

To evaluate the energetic contribution of each mode to the stability of the polar structure, we plot the change in total energy as a function of mode amplitude frozen into the paraelectric reference phase in Fig. 2. Consistent with

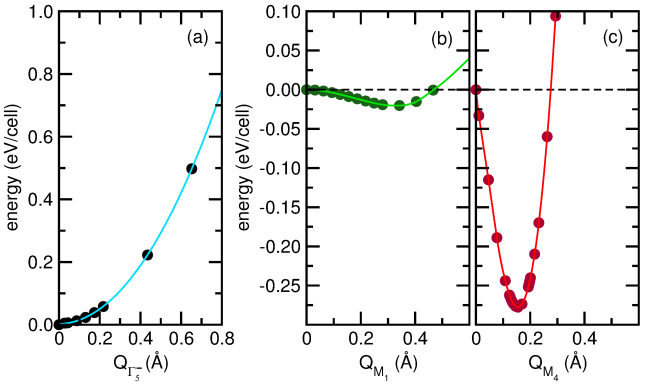

FIG. 2. Relative energy of LSMO for increasing amplitude of the (a) polar ($Q_{\Gamma_5^-}$), (b) rotation (Q_{M_1}) and (c) Jahn-Teller (Q_{M_4}) distortions. Independent of other modes, only the antiferrodistortive (b) and (c) modes are energetically favorable.

our phonon calculations, the polar $Q_{\Gamma_5^-}$ mode is stable, while the octahedral rotation Q_{M_1} mode is weakly unstable and leads to a modest energy gain of approximately 20 meV per cell at its optimal amplitude. On the other hand, the dynamically stable Jahn-Teller distortion described by Q_{M_4} does lower the energy of the system: We observe a large energy stabilization at finite amplitude of the Jahn-Teller distortion, which corresponds to Mn–O equatorial bonds of approximately 1.88 and 2.04 Å within each MnO_6 octahedron. The two-dimensional Q_{M_4} mode displaces such oxygen sites, generating a "two-in–two-out" cooperative pattern of the Mn–O equatorial bonds while it leaves unaltered the position of the apical oxygen atoms (Fig. 3a).

In the case of the Jahn-Teller distortion, the energy does not exhibit quadratic behavior with respect to the Q_{M_4} distortion amplitude (Fig. 2c). For small amplitude, the energy evolution is linear. Such terms, however, are not permitted[46] in the Landau free energy for $P4/nmm$ $LaSrMnO_4$ expanded in Q_{M_4} as the order parameter:

$$\mathcal{F}(Q_{M_4}) \simeq \alpha Q_{M_4}^2 + \beta Q_{M_4}^4 + \gamma Q_{M_4} + \delta Q_{M_4}^3. \quad (1)$$

The energetic dependence of the displacive Q_{M_4} mode appears to make it a poor order parameter in $LaSrMnO_4$, provided that the system should be well-described within Landau theory, *i.e.*, $\gamma = \delta = 0$.

An alternative order-parameter which captures the physics of the FOJT may remedy this apparent inconsistency. Owing to the importance of the Jahn-Teller mode in preferentially stabilizing various radial symmetry d-orbitals, we calculate the electronic orbital polarization $\mathcal{P}$ of the Mn e_g orbitals as a function of the Q_{M_4} mode amplitude (Fig. 3b).[47] We first note that the Q_{M_4} mode enforces that there is only one Mn crystallographic site in the structure upon distortion (Wyckoff position 4c); in addition, when $Q_{M_4} = 0$ all Mn sites are structurally equivalent. Indeed, we find at $Q_{M_4} = 0$, the orbital polarization for all Mn atoms is identical ($\sim -3.8\%$). Interestingly, when we compute $\mathcal{P}$ for each of the four Mn

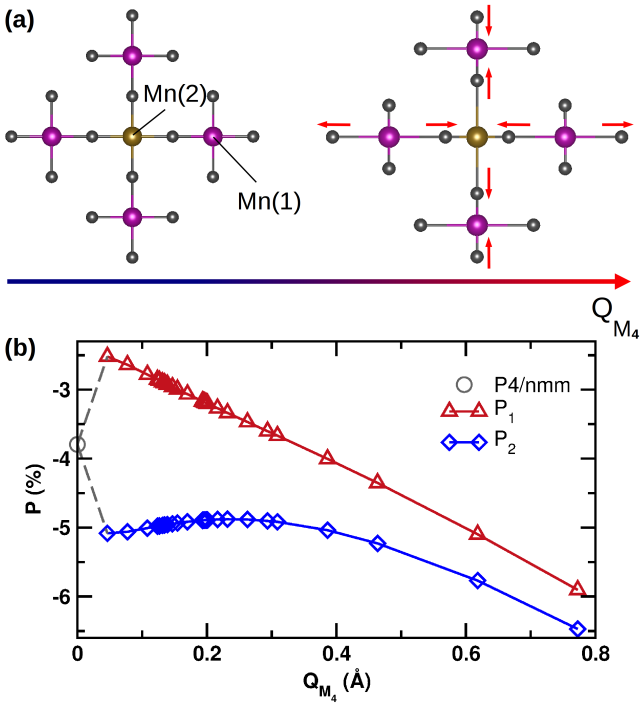

FIG. 3. (a) Schematic illustration of the Jahn-Teller distortion (Q_{M_4}), which alters only the equatorial oxygen atoms in the ab plane. The model also mediates the interaction between two nearest-neighbor Mn sites. (b) Orbital polarization of Mn(1) ($\mathcal{P}_1$) and Mn(2) ($\mathcal{P}_2$) polarization sites against Jahn-Teller distortion mode amplitude. In the presence of Q_{M_4} distortion, the Mn crystallographic site is equivalent but the Mn e_g polarization is site-dependent. Both $\mathcal{P}_1$ and $\mathcal{P}_2$ polarizations are equivalent at zero distortion amplitude (gray open circle), when the structure has the $P4/nmm$ symmetry. At high distortion values, Mn(1)–Mn(2) coupling is removed.

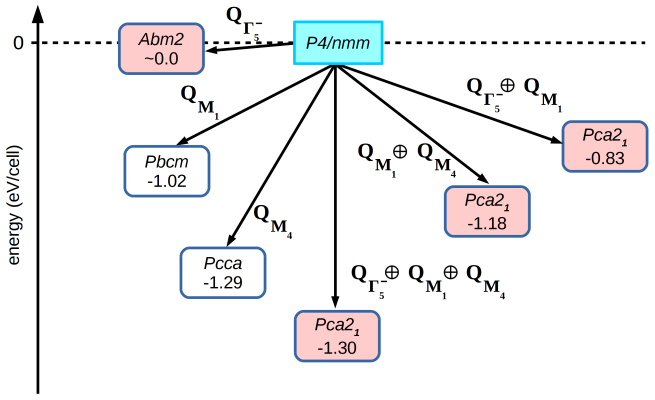

FIG. 4. Group-subgroup relations with calculated energy stabilities for ordered $LaSrMnO_4$ fully relaxed within the specified symmetry. The structural transition $P4/nmm \rightarrow Pca2_1$ can be realized by coupling at least two of the $Q_{\Gamma_5^-}$, Q_{M_1}, and Q_{M_4} distortions. Shaded (pink) boxes with rounded corners indicate polar symmetries.

atoms at values of $Q_{M_4} \neq 0$, we find two distinct Mn cations within the same MnO_2 plane can be differentiated according to their respective $\mathcal{P}_1$ and $\mathcal{P}_2$ orbital polarizations (Fig. 3b). We refer to the Mn cations with distinct orbital polarizations as Mn(1) and Mn(2) (see Fig. 1b).

The Mn-site orbital polarizations show a peculiar trend with respect to the Q_{M_4} amplitude. $\mathcal{P}_1$ decreases linearly with increasing amplitude of the Jahn-Teller distortion, whereas $\mathcal{P}_2$ has a parabolic behavior for $Q_{M_4} \lesssim 0.4$ Å, becoming asymptotically linear at higher distortion amplitudes. Note that in the ground state $Q_{M_4} = 0.15$ Å, which is well below this transition point. To understand this behavior, it is important to recall that within each two-dimensional MnO_2 layer, two nearest-neighbor Mn sites are connected through one of the equatorial oxygen atoms. This ligand behaves as a "bridging atom" for which electronic charge can flow. At high Q_{M_4} mode-distortion amplitudes, the Mn–O bonds are stretched in such a way that the $2p$ orbitals of each bridging oxygen atom effectively only hybridized with one of the two nearest neighbor Mn atoms. As a consequence, $\mathcal{P}_2$ has a linear trend when such configuration is realized, suggesting that the parabolic behavior at low Q_{M_4} amplitudes results from a charge transfer between sites owing to a Mn(1)–Mn(2) interaction occurring through the bridging oxygen atoms, *i.e.*, $\mathcal{P}_1$ decreases as $\mathcal{P}_2$ increases. We note that if the Q_{M_4} distortion is reversed, then the role of the Mn(1) and Mn(2) cation sites as we have identified them would also switch owing to a Jahn-Teller pseudo-rotation symmetry operation as already observed in certain metalorganic multiferroic materials.[48]

According to the symmetry of the system, the Landau potential should contain only even powers of the order parameters (*e.g.*, $Q_{\Gamma_5^-}$, Q_{M_1} and Q_{M_4}); however, we find that within this parameter space the free energy would require odd powers of Q_{M_4}. We reconcile this issue by involving the coupling of the local Mn orbital polarizations. The free energy $\mathcal{F}$ in Equation 1 can be rewritten in terms of the $\mathcal{P}_1$ and $\mathcal{P}_2$ local orbital polarizations, taking into account the coupling $\mathcal{P}_1 \cdot \mathcal{P}_2$ between the two Mn polarization sites; this term is symmetry allowed and it replaces the forbidden linear and cubic Q_{M_4} terms.[49]

2. *Coupled Distortions*

Since octahedral rotations and Jahn-Teller distortion are both found to be energetically favored, we calculate the change in energy for $LaSrMnO_4$ in the presence of both distortions at different amplitudes. The fourth order Landau energy expansion fits the energy trend, confirming that the Q_{M_1}, and Q_{M_4} coupling is favored and both kinds of distortion cooperate to lower the system energy (not shown).

We also tested the energetic stability of different coupled lattices modes, allowing for full ionic relaxation within the symmetry generated by the coupled modes (Fig. 4). Among the structures with $Pca2_1$ symmetry, as anticipated, the one with lowest energy is realized only when all the three $Q_{\Gamma_5^-}$, Q_{M_1} and Q_{M_4} distortions are

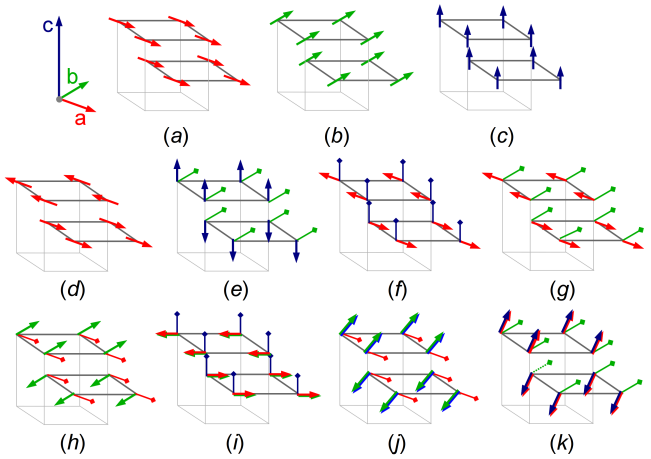

FIG. 5. Stable magnetic configurations calculated for the $Pca2_1$ ground phase. Each arrow is centered on a Mn site: the color represents the direction of the magnetic component corresponding to the crystallographic axis shown in the upper left. (a)-(c): ferromagnetic orderings. (d): antiferromagnetic ordering LA_a. (e)-(k): antiferromagnetic ordering with weak ferromagnetic component M_i; arrows terminated with a diamond correspond to the weak ferromagnetic component while solid shaded arrows in (i)-(k) correspond to the main magnetic component lying in the (ab), (bc) and (ac) plane, respectively.

present. Since the Γ_5^- mode alone is stable, its presence in the polar phase may be explained by considering higher order anharmonic interactions of the kind $Q^2_{\Gamma_5^-}Q^2_{M_1}Q^2_{M_4}$ in the energy expansion, corresponding to the ($Q_{\Gamma_5^-}$,Q_{M_1},Q_{M_4}) coupling allowed by symmetry. The ferroelectric distortion thus appears in the ground phase owing to the presence and coupling between octahedral rotations and Jahn-Teller distortions; these two *centric* modes are therefore responsible for lifting inversion symmetry.

C. Ferroic Properties

The calculated macroscopic electric polarization P for $LaSrMnO_4$ is $1.25\,\mu C\,cm^{-2}$ and oriented along the a axis. As noted earlier, the polar ground state can be realized without condensation of the $Q_{\Gamma_5^-}$ mode. The anharmonic interaction between the octahedral rotations and the Jahn-Teller mode sufficiently reduce the symmetry to allow for an electric polarization to arise. Using the equilibrium geometries for the octahedral rotation and Jahn-Teller modes but without including the $Q_{\Gamma_5^-}$ displacements, we compute an electric polarization of $0.70\,\mu C\,cm^{-2}$. In the other case, if only the polar $Q_{\Gamma_5^-}$ displacements are present, we obtain a $0.55\,\mu C\,cm^{-2}$ polarization. We thus conclude that the cation ordered $LaSrMnO_4$ is a hybrid-improper ferroelectric.

The symmetries of the $LaSrMnO_4$ structure allow trilinear terms of the type $M_iP_jLA_k$, representing the coupling between the weak FM component M, the polarization P, and AFM ordering LA along the crystallographic a, b and c directions, respectively. We explored the interactions between these spin and electric degrees of freedom by relaxing different starting non-collinear spin orientations keeping fixed the previously optimized $Pca2_1$ geometry (Fig. 5). All explored magnetic configurations (Table I) are found to be stable with small energy differences irrespective of the particular configuration considered (∼50 μeV), with the collinear AFM A-type configuration being most stable (Fig. 1c and Fig. 5d).

TABLE I. Calculated components of the total magnetization $\mathbf{M}$ (μ_B per cell) and permitted (forbidden) directions of the weak-ferromagnetic M_i and anti-ferromagnetic LA_k components specified by a × (·) symbol for the 11 magnetic spin configurations (Conf.). Note that one cell contains four Mn cations.

Conf.[a]	$\mathbf{M}_a$	$\mathbf{M}_b$	$\mathbf{M}_c$	M_a	M_b	M_c	LA_a	LA_b	LA_c
a	15.5	0.0	0.0	·	·	·	·	·	·
b	0.0	15.5	0.0	·	·	·	·	·	·
c	0.0	0.0	15.5	·	·	·	·	·	·
d	0.0	0.0	0.0	·	·	·	×	·	·
e	0.0	3.8	0.0	·	×	·	·	·	×
f	3.8	0.0	0.0	·	·	×	×	·	·
g	0.0	3.8	0.0	·	×	·	×	·	·
h	3.8	0.0	0.0	×	·	·	·	×	·
i	0.0	0.0	3.7	·	·	×	×	×	·
j	3.7	0.0	0.0	×	·	·	·	×	×
k	0.0	3.7	0.0	·	×	·	×	·	×

[a] Graphical spin structure representations are given in Fig. 5.

To obtain more detailed information on the effect of the spin arrangement on the electronic structure, the Mn-O bond covalency has been analyzed with the definition previously applied for the prototypical $CaFeO_3$ perovskite.[50] Consistent with total energy differences among the considered magnetic configurations, the electronic distribution along the Mn–O bond is weakly affected by the particular magnetic arrangement. The bond covalency is mainly determined by the Mn–O interatomic distances, revealing that the electronic configuration of the relaxed $Pca2_1$ phase is stable against changes to the static spin-density distribution.

Owing to the small energy differences among the various spin configurations, we are unable to conclusively establish the nature of the magnetic structure of the polar phase. This behavior is likely a consequence of the layered structure, with weak interlayer MnO_2 interactions. The small energy separation among the different magnetic configurations are compatible with both a paramagnetic and a spin density wave description of the magnetic ground state. Further investigations on $LaSrMnO_4$ should aim to uncover its magnetoelectric properties, examining which centric mode is responsible for switching the polarization and weak-ferromagnetic order via the allowed $M_iP_jLA_k$ invariants.

IV. CONCLUSIONS

In summary, we have shown that the $LaSrMnO_4$ Ruddlesden-Popper phase with cation ordering undergoes a ferroelectric transition $P4/nmm \rightarrow Pca2_1$ owing to the cooperative effect of octahedral rotations and Jahn-Teller distortion modes. The Jahn-Teller distortions stabilize the system through changes to the e_g orbital polarizations of two nearest neighbor Mn sites. The octahedral rotations are dynamically unstable in the paraelectric phase and together with the Jahn-Teller distortion stabilize the polar phase, making $LaSrMnO_4$ a hybrid-improper ferroelectric with a $1.25\,\mu C\,cm^{-2}$ electric polarization. Analysis of the different magnetic configurations explored in this work shows that our computational description of the $Pca2_1$ polar phase is compatible with either a paramagnetic or SDW structure. Owing to the non-collinear spin structure and weak-ferromagnetism, magnetoelectric coupling is permitted in cation ordered $LaSrMnO_4$. Further computational studies are required to clarify the strength of the magnetoelectric response. We hope this work motivates the experimental synthesis of cation ordered Ruddelsden-Popper structures.

ACKNOWLEDGMENTS

A.C. acknowledges support by the European social fund within the framework of the project "Support of inter-sectoral mobility and quality enhancement of research teams at Czech Technical University in Prague" (CZ.1.07/2.3.00/30.0034). J.M.R. was supported by the U.S. Office of Naval Research, under grant number N00014-11-1-0664. Both authors thank A. Stroppa and P.V. Balachandran for useful discussions. This work used the Extreme Science and Engineering Discovery Environment (XSEDE), which is supported by National Science Foundation under grant number OCI-1053575, and the Carbon cluster hosted at the Center for Nanoscale Materials which is supported by the U.S. Department of Energy, Office of Science, Office of Basic Energy Sciences, under Contract No. DE-AC02-06CH11357. The use of VESTA software[51] is also acknowledged.

* cammaant@fel.cvut.cz
† jrondinelli@northwestern.edu

[1] T. Kimura, T. Goto, H. Shintani, K. Ishizaka, T. Arima, and Y. Tokura, Nature **426**, 55 (2003).
[2] S. W. Cheong and M. Mostovoy, Nat. Mater **6**, 13 (2007).
[3] A. Filippetti and N. A. Hill, Phys. Rev. B **65**, 195120 (2002).
[4] D. V. Efremov, J. van den Brink, and D. I. Khomskii, Nat Mater **3**, 853 (2004).
[5] I. B. Bersuker, Phys. Rev. Lett. **108**, 137202 (2012).
[6] T. Kimura, Ann. Rev. Mat. Res. **337**, 387 (2007).
[7] J. Brink and D. Khomskii, J. Phys: Condens. Mat. **20**, 434217 (2008).
[8] F. Kagawa, S. Horiuchi, M. Tokinaga, J. Fujioka, and Y. Tokura, Nature Phys. **6**, 169 (2010).
[9] J. M. Perez-Mato, M. Aroyo, A. García, P. Blaha, K. Schwarz, J. Schweifer, and K. Parlinski, Phys. Rev. B **70**, 214111 (2004).
[10] J. M. Perez-Mato, P. Blaha, K. Schwarz, M. Aroyo, D. Orobengoa, I. Etxebarria, and A. García, Phys. Rev. B **77**, 184104 (2008).
[11] N. A. Benedek, A. T. Mulder, and C. J. Fennie, Journal of Solid State Chemistry **195**, 11 (2012).
[12] N. A. Benedek, J. M. Rondinelli, H. Djani, P. Ghosez, and P. Lightfoot, Dalton Trans. , Advance Article (2015).
[13] E. Bousquet, M. Dawber, N. Stucki, C. Lichtensteiger, P. Hermet, S. Gariglio, J.-M. Triscone, and P. Ghosez, Nature **452**, 732 (2008).
[14] P. Ghosez and J.-M. Triscone, Nat Mater **10**, 269 (2011).
[15] L. Bellaiche and J. Íñiguez, Phys. Rev. B **88**, 014104 (2013).
[16] T. Fukushima, A. Stroppa, S. Picozzi, and J. M. Perez-Mato, Phys. Chem. Chem. Phys. **13**, 12186 (2011).
[17] N. A. Benedek and C. J. Fennie, Phys. Rev. Lett. **106**, 107204 (2011).
[18] Y. Krockenberger, K. Mogare, M. Reehuis, M. Tovar, M. Jansen, G. Vaitheeswaran, V. Kanchana, F. Bultmark, A. Delin, F. Wilhelm, A. Rogalev, A. Winkler, and L. Alff, Phys. Rev. B **75**, 020404 (2007).
[19] J. Alaria, P. Borisov, M. S. Dyer, T. D. Manning, S. Lepadatu, M. G. Cain, E. D. Mishina, N. E. Sherstyuk, N. A. Ilyin, J. Hadermann, D. Lederman, J. B. Claridge, and M. J. Rosseinsky, Chem. Sci. **5**, 1599 (2014).
[20] A. J. Millis, Nature **392**, 147 (1998).
[21] T. Goto, T. Kimura, G. Lawes, A. P. Ramirez, and Y. Tokura, Phys. Rev. Lett. **92**, 257201 (2004).
[22] M. Rini, R. Tobey, N. Dean, J. Itatani, Y. Tomioka, Y. Tokura, R. W. Schienlein, and A. Cavalleri, Nature **449**, 72 (2007).
[23] M. A. Carpenter and C. J. Howard, Acta Crystallographica Section B **65**, 134 (2009).
[24] M. A. Carpenter and C. J. Howard, Acta Crystallographica Section B **65**, 147 (2009).
[25] E. K. H. Salje and M. A. Carpenter, Journal of Physics: Condensed Matter **23**, 462202 (2011).
[26] J. Varignon, N. C. Bristowe, E. Bousquet, and P. Ghosez, ArXiv e-prints (2014), arXiv:1409.8422 [cond-mat.mtrl-sci].
[27] A. Stroppa, P. Barone, P. Jain, J. M. Perez-Mato, and S. Picozzi, Adv. Mater. **25**, 2284 (2013).
[28] D. Di Sante, A. Stroppa, P. Jain, and S. Picozzi, Journal of the American Chemical Society **135**, 18126 (2013).
[29] A. O. Polyakov, A. H. Arkenbout, J. Baas, G. Blake, A. Meetsma, A. Caretta, P. vanLoosdrecht, and T. Palstra, Chem. Mater. **24**, 133 (2011).
[30] R. Gautier, X. Zhang, L. Hu, L. Yu, Y. Lin, S. O. L., D. Chon, K. R. Poeppelmeier, and A. Zunger, Nat. Chem. **7**, 308 (2015).
[31] A. Gössling, M. W. Haverkort, M. Benomar, H. Wu, D. Senff, T. Möller, M. Braden, J. A. Mydosh, and M. Grüninger, Phys. Rev. B **77**, 035109 (2008).

[32] S. Larochelle, A. Mehta, L. Lu, P. K. Mang, O. P. Vajk, N. Kaneko, J. W. Lynn, L. Zhou, and M. Greven, Phys. Rev. B **71**, 024435 (2005).

[33] P. Reutler, O. Friedt, B. Bchner, M. Braden, and A. Revcolevschi, Journal of Crystal Growth **249**, 222 (2003).

[34] M. Vafaee, M. Baghaie Yazdi, A. Radetinac, G. Cherkashinin, P. Komissinskiy, and L. Alff, Journal of Applied Physics **113**, 053906 (2013).

[35] B. B. Nelson-Cheeseman, A. B. Shah, T. S. Stantos, J. M. Zuo, and A. Bhattacharya, Appl. Phys. Lett. **98**, 072505 (2011).

[36] B. B. Nelson-Cheeseman, H. Zhou, P. V. Balachandran, G. Fabbris, J. Hoffman, D. Haskel, J. M. Rondinelli, and A. Bhattacharya, Advanced Functional Materials **24**, 6884 (2014).

[37] P. V. Balachandran, D. Puggioni, and J. M. Rondinelli, Inorganic Chemistry **53**, 336 (2014).

[38] P. V. Balachandran, A. Cammarata, B. B. Nelson-Cheeseman, A. Bhattacharya, and J. M. Rondinelli, APL Materials **2**, 076110 (2014).

[39] P. E. Blöchl, Phys. Rev. B **50**, 17953 (1994).

[40] G. Kresse and J. Furthmller, Computational Materials Science **6**, 15 (1996); G. Kresse and D. Joubert, Phys. Rev. B **59**, 1758 (1999).

[41] V. I. Anisimov, F. Aryasetiawan, and A. I. Lichtenstein, Journal of Physics: Condensed Matter **9**, 767 (1997).

[42] A. I. Liechtenstein, V. I. Anisimov, and J. Zaanen, Phys. Rev. B **52**, R5467 (1995).

[43] J. M. Perez-Mato, D. Orobengoa, and M. I. Aroyo, Acta Crystallographica Section A **66**, 558 (2010).

[44] B. J. Campbell, H. T. Stokes, D. E. Tanner, and D. M. Hatch, J. Appl. Cryst. **39**, 607 (2006).

[45] S. Yarlagadda, P. B. Littlewood, M. Mitra, and R. K. Monu, Phys. Rev. B **80**, 235123 (2009).

[46] L. D. Landau and E. M. Lifshitz, *Statistical Physics Part 1 (Third Edition)* (Pergamon, New York, 1980) §145.

[47] The e_g orbital polarization is computed as described in A. Cammarata and J. M. Rondinelli, Phys. Rev. B **87**, 155135 (2013), and is defined as $\mathcal{P} = \frac{n[d(x^2-y^2)]-n[d(3z^2-r^2)]}{n[d(x^2-y^2)]+n[d(3z^2-r^2)]}$, where $n[d(x^2-y^2)]$ and $n[(d_{3z^2-r^2})]$ are the occupancies of the $d(x^2-y^2)$ and $d(3z^2-r^2)$ orbitals, respectively.

[48] A. Stroppa, P. Jain, P. Barone, M. Marsman, J. M. Perez-Mato, A. K. Cheetham, H. W. Kroto, and S. Picozzi, Angew. Chem. Int. Ed. **50**, 5847 (2011).

[49] The free energy $\mathcal{F}$, restated in terms of the $\mathcal{P}_1$ and $\mathcal{P}_2$ local orbital polarizations, has the following expression:

$$\mathcal{F}(Q_{M_4}, \mathcal{P}) = \tilde{\alpha} Q_{M_4}^2 + \tilde{\beta} Q_{M_4}^4 + \tilde{\gamma}(\mathcal{P}_1 \cdot \mathcal{P}_2).$$

The expression above contains only symmetry allowed terms. The product $\mathcal{P}_1 \cdot \mathcal{P}_2$ is invariant under symmetry operations, despite the linear $\mathcal{P}_1$ and $\mathcal{P}_2$ local polarization terms not being permitted. The coupling term $\mathcal{P}_1 \cdot \mathcal{P}_2$ takes into account the linear and the parabolic behavior of $\mathcal{P}_1$ and $\mathcal{P}_2$, respectively:

$$\mathcal{P}_1 \cdot \mathcal{P}_2 = (a + bQ_{M_4}) \cdot (c + dQ_{M_4} + eQ_{M_4}^2).$$

In this way, the free energy expansion $\mathcal{F}$ now contains also linear and cubic terms of the Q_{M_4} distortion amplitude, reproducing correctly the energy trend shown in Fig. 2 and providing a second-order transition description of the symmetry reduction.

[50] A. Cammarata and J. M. Rondinelli, J. Chem. Phys. **141**, 114704 (2014).

[51] K. Momma and F. Izumi, Journal of Applied Crystallography **41**, 653 (2008).